

BEM analysis of semipermeable piezoelectric cracks

M. Denda

Rutgers University

Mechanical and Aerospace Engineering Department

98 Brett Road, Piscataway, New Jersey 08854-8058, U.S.A.

Abstract

A boundary element method (BEM) for the analysis of the semipermeable crack is developed using the numerical Green's function approach. The extended crack opening displacement (COD) of a straight crack is represented by the continuous distribution of extended dislocation dipoles, with the built-in \sqrt{r} COD behavior, which is integrated analytically to give the whole crack singular element (WCSE) equipped with the \sqrt{r} COD and the $1/\sqrt{r}$ crack tip extended stress singularity. Linear BEM solvers for the impermeable and permeable cracks are developed first and then an iterative procedure to reach the semipermeable solution using the impermeable and permeable solvers is proposed. The convergence study is performed for the single cracks in the infinite and finite bodies with associated numerical results for the extended stress intensity factors (SIFs) and other variables. The proposed numerical Green's function approach does not require the post-processing for the accurate determination of the extended stress intensity factors and is ideally suited for the proposed nonlinear iteration scheme for the semipermeable cracks.

Keywords: Piezoelectricity, Electrically Semipermeable Crack, Boundary Element Method, Numerical Green's Function

1. Introduction

The electric boundary condition (BC) on the piezoelectric crack surface comes in different degrees of shielding the electric induction defined by the electric permeability. The permeable crack along

the x_1 -axis given by the BC,

$$D_2^+ = D_2^-; \quad \Phi^+ - \Phi^- = 0, \quad (1)$$

does not shield the electric induction at all, where D_2 and Φ are the electric induction and the electric potential, respectively, with \pm indicating the upper and lower crack surfaces. The impermeable crack with the BC,

$$D_2^+ = D_2^- = 0, \quad (2)$$

shields the electric induction completely. If the crack is closed, then the permeable BC is correct, while the impermeable BC is correct if the permittivity ε_c of the crack medium is zero. Since there is no medium with zero permittivity (the vacuum has the least permittivity $\varepsilon_{air} = 8.854 \times 10^{-12} C/Vm$), the two boundary conditions are not correct for opened cracks. Narita et al. [1] reports that results predicted by the permeable BC are in much better agreement with the experimental results than those by the impermeable BC. If the crack opening displacement is extremely small, as in the typical piezoceramic specimens, the permeable BC may provide a good approximation despite its inconsistency. The semipermeable BC,

$$D_2^+ = D_2^-; \quad D_2^+(u_2^+ - u_2^-) = -\varepsilon_c(\Phi^+ - \Phi^-), \quad (3)$$

proposed by Hao and Shen [2] gives the consistent BC for opened cracks. Recall that the semipermeable BC is reduced to the impermeable BC when $\varepsilon_c = 0$ and to the permeable BC when $u_2^+ - u_2^- = 0$ and that the impermeable and permeable BCs set the bounds for the semipermeable BC. Due to the convenience to obtain the analytical solution, the majority of the earlier works adopted the impermeable BC ([3], [4], [5], [6], [7], [8], [9], [10], [11], [12], [13], [14], [15], [16], [17], [18], [19], [20], [21], [22], [23]) and the permeable BC ([24], [25], [26], [27], [28], [1]). The progress toward the consistent semipermeable BC was made gradually but slowly ([2], [29], [30], [31], [32], [33], [34], [35],[36],[37],[38]). Zhang et al. [39], [36] considered the crack to be the limit of an elliptical hole to derive three BCs described above and clearly identified the relations among them.

This paper adopts the the numerical Green's function approach, developed by Denda and Mansukh [40], based on the whole crack singular element (WCSE) for the general piezoelectric solids in two-dimensions for impermeable and permeable BCs. The extended crack opening displacement (COD) of the straight crack is represented by the continuous distribution of extended dislocation dipoles, with the embedded \sqrt{r} COD behavior, which is integrated analytically to give the \sqrt{r} COD and the $1/\sqrt{r}$ crack tip extended stress singularity. While the FEM needs to model the entire domain surrounding a crack, the BEM using the WCSE only needs a single line to model the crack.

In addition, the proposed numerical Green's function approach does not require the post-processing for the accurate determination of the extended stress intensity factors (SIFs). It makes more sense to use the BEM for crack problem.

While the solutions of the permeable and the impermeable cracks are linear, that of the semipermeable crack is nonlinear. Since the distribution of the electric induction on the crack surface, which is needed to determine the crack opening displacement and the electric potential jump across the crack, is unknown we need an iteration process to determine all unknowns. This is inherently a nonlinear process even though each step consists of the linear solver. We propose an iteration scheme to achieve the semipermeable BC using the linear solution procedure by the boundary element method (BEM) developed for permeable and impermeable cracks. The convergence of the iteration is studied for various single crack configurations and the extended stress intensity results are reported.

2. Basic Equations for Piezoelectricity

2.1. Piezoelectric equations in 3-D

For the piezoelectric solids strain (ϵ_{ij}) and electric (E_i) fields in three-dimensions are related to the stress (σ_{kl}) and electric induction (D_k) fields by the equations,

$$\begin{aligned} \epsilon_{ij} &= s_{ijkl}\sigma_{kl} + g_{kij}D_k, \\ E_i &= -g_{ikl}\sigma_{kl} + \beta_{ik}D_k, \end{aligned} \quad (4)$$

where s_{ijkl} , g_{ikl} , β_{ik} are the elastic compliance, piezoelectric, and dielectric impermeability constants, respectively. Introduce the extended strain and stress,

$$\langle \mathcal{E}_{Ij}, \Sigma_{Ij} \rangle = \begin{cases} \langle \epsilon_{ij}, \sigma_{ij} \rangle & (I \equiv i = 1, 2, 3) \\ \langle E_j, D_j \rangle & (I = 4) \end{cases}, \quad (5)$$

for $j = 1, 2, 3$ and the extended compliance constants,

$$\mathcal{S}_{IjKl} = \begin{cases} s_{ijkl} & (I \equiv i = 1, 2, 3; K \equiv k = 1, 2, 3) \\ g_{lij} & (K = 4; I \equiv i = 1, 2, 3) \\ -g_{jkl} & (I = 4; K \equiv k = 1, 2, 3) \\ \beta_{jl} & (I = K = 4) \end{cases}, \quad (6)$$

to give the concise extended strain and stress relations,

$$\mathcal{E}_{Ij} = \mathcal{S}_{IjKl}\Sigma_{Kl}, \quad (7)$$

replacing (4). The lower and upper case Roman indices range from 1 to 3 and 1 to 4, respectively. The repeated index is summed over its respective range unless mentioned otherwise. The extended displacement, point force, and traction are defined by

$$\langle U_I, F_I, T_I \rangle = \begin{cases} \langle u_i, f_i, t_i \rangle & (I \equiv i = 1, 2, 3) \\ \langle \phi, -\rho_e, -\omega_e \rangle & (I = 4) \end{cases}, \quad (8)$$

where u_i and φ are the displacement and electric potential, f_i and ρ_e are the body force and charge density components, and t_i and ω_e are the traction and surface charge density components.

The extended equilibrium equations, consisting of the force equilibrium equations and the Gauss's law, are given by

$$\Sigma_{Ij,j} + F_I = 0, \quad (9)$$

where a comma followed by a subscript j indicates the differentiation by the coordinate x_j . The extended strain is given by

$$\mathcal{E}_{Ij} = \begin{cases} \frac{1}{2}(U_{i,j} + U_{j,i}) & (I \equiv i = 1, 2, 3) \\ -U_{I,j} & (I = 4) \end{cases} \quad (10)$$

for $j = 1, 2, 3$ and the extended traction by

$$T_I = \Sigma_{Ij}n_j, \quad (11)$$

where n_j is the unit normal component of the surface element.

2.2. Piezoelectric Equations in 2-D

In the plane piezoelectricity problem the extended displacement components depend only on two coordinates x_1 and x_2 . The pair of suffices ij , appearing in the stress, strain and compliance components, are replaced by a single suffix \mathcal{M} according to the convention (11 \rightarrow 1), (22 \rightarrow 2), (33 \rightarrow 3), (23 \rightarrow 4), (31 \rightarrow 5), (12 \rightarrow 6). Note that the suffices for the electric and electric induction fields and the corresponding indices for the piezoelectric and dielectric impermeability constants are not reduced. The strain components are given by

$$e_1 = u_{1,1}, \quad e_2 = u_{2,2}, \quad e_4 = u_{3,2}, \quad e_5 = u_{3,1}, \quad e_6 = u_{2,1} + u_{1,2}, \quad (12)$$

and the electric field components by

$$E_1 = -\phi_{,1} \quad E_2 = -\phi_{,2}. \quad (13)$$

The compatibility equations are given by

$$\begin{aligned} e_{2,11} + e_{1,22} - e_{6,12} &= 0, & e_{4,1} - e_{5,2} &= 0, \\ E_{2,1} - E_{1,2} &= 0. \end{aligned} \quad (14)$$

Since $e_3 = E_3 \equiv 0$ the stress and electric induction components σ_3 and D_3 can be eliminated from (4) to give the reduced extended strain and stress relations

$$\begin{aligned} e_{\mathcal{M}} &= S_{\mathcal{M}\mathcal{N}} \sigma_{\mathcal{N}} + G_{\alpha\mathcal{M}} D_{\alpha}, \\ E_{\alpha} &= -G_{\alpha\mathcal{N}} \sigma_{\mathcal{N}} + B_{\alpha\gamma} D_{\gamma}, \end{aligned} \quad (15)$$

in terms of the reduced elastic compliance $S_{\mathcal{M}\mathcal{N}}$, piezoelectric constants $G_{\alpha\mathcal{N}}$ and dielectric impermeability constants $B_{\alpha\beta}$ (Denda and Mansukh [40]). The Greek index ranges from 1 to 2 and the comma followed by a subscript α indicates differentiation by x_{α} .

In the extended Stroh formalism for 2D piezoelectricity the extended displacement U_I , stress function Ψ_I , and the stress components $\Sigma_{I\alpha}$ are given in the form

$$\begin{aligned} U_I &= 2\Re\left\{\sum_{J=1}^4 A_{IJ} f_J(z_J)\right\}, & \Psi_I &= 2\Re\left\{\sum_{J=1}^4 L_{IJ} f_J(z_J)\right\}, \\ \Sigma_{I2} &= \frac{\partial \Psi_I}{\partial x_1} = 2\Re\left\{\sum_{J=1}^4 L_{IJ} f'_J(z_J)\right\}, \\ \Sigma_{I1} &= -\frac{\partial \Psi_I}{\partial x_2} = -2\Re\left\{\sum_{J=1}^4 \eta_J L_{IJ} f'_J(z_J)\right\}, \end{aligned} \quad (16)$$

where the symbols \Re and \Im indicate the real and imaginary parts of a complex number and A_{IJ} and L_{IJ} are 4×4 complex valued matrix and η_J ($J = 1, \dots, 4$ with $\Im(\eta_J) > 0$) are the roots of the eighth order characteristic polynomial originating from the compatibility equation (14). The characteristic roots are assumed to be distinct and the degenerate cases of coincident roots can be treated by slightly perturbing the material constants to make all roots distinct. The functions $f_J(z_J)$ ($J = 1, \dots, 4$) are analytic functions of the generalized complex variables $z_J = x_1 + \eta_J x_2$ ($J = 1, \dots, 4$) and $f'_J(z_J) = df_J(z_J)/dz_J$. The details on the characteristic equations and the matrices L_{IJ} and A_{IJ} can be found in Denda and Mansukh [40].

3. Direct formulation of the Piezoelectric BEM

The basis of the direct formulation of the boundary element method for piezoelectricity is the extended Somigliana's identity,

$$U_K(\mathbf{x}) = \int_{\partial A} T_I(\mathbf{y}) G_{IK}(\mathbf{y}-\mathbf{x}) dl(\mathbf{y}) - \int_{\partial A} U_I(\mathbf{y}) H_{IK}(\mathbf{y}-\mathbf{x}; \mathbf{v}) dl(\mathbf{y}), \quad (17)$$

where $G_{IK}(\mathbf{x})$ is the fundamental solution with the physical interpretations:

$G_{ik}(\mathbf{x})$: elastic displacement in the x_i -direction at \mathbf{x} due to a line force in the x_k -direction at the origin;

$G_{i4}(\mathbf{x})$: elastic displacement in the x_i -direction at \mathbf{x} due to a line charge at the origin;

$G_{4k}(\mathbf{x})$: electric potential at \mathbf{x} due to a line force in the x_k -direction at the origin; and

$G_{44}(\mathbf{x})$: electric potential at \mathbf{x} due to a line charge at the origin.

The kernel $H_{IK}(\mathbf{y}-\mathbf{x}; \mathbf{v})$ is the I th component of the extended traction at \mathbf{y} corresponding to the extended line force in the x_K -direction at \mathbf{x} and given by

$$H_{IK}(\mathbf{y}-\mathbf{x}; \mathbf{v}) = v_\alpha(\mathbf{y}) E_{\alpha IP\beta} G_{PK,\beta}(\mathbf{y}-\mathbf{x}), \quad (18)$$

where $v_\alpha(\mathbf{y})$ is the unit normal component on the boundary ∂A .

According to the physical interpretation of the extended Somigliana's identity (Denda and Mansukh [40]), the extended displacement field in a domain A can be represented by continuous distributions of the extended line forces (T_I) and dislocation dipoles (U_I) along the contour ∂A in an infinite body that coincides with the boundary of the domain, where T_I and U_I are the magnitudes of the extended traction and displacement on the boundary. This physical interpretation gives the extended Somigliana's identity in an alternative form

$$U_K(\mathbf{x}) = \int_{\partial A} G_{KI}(\mathbf{x}-\mathbf{y}) T_I(\mathbf{y}) dl(\mathbf{y}) + \int_{\partial A} H_{KI}(\mathbf{x}-\mathbf{y}; \mathbf{v})^* U_I(\mathbf{y}) dl(\mathbf{y}), \quad (19)$$

where $H_{KI}(\mathbf{x}-\mathbf{y}; \mathbf{v})^* dl(\mathbf{y}) = -H_{IK}(\mathbf{y}-\mathbf{x}; \mathbf{v}) dl(\mathbf{y})$ is the extended displacement in the x_K -direction at \mathbf{x} due to the extended dislocation dipole at \mathbf{y} with the unit discontinuity in the x_I -direction, which occurs along the segment $dl(\mathbf{y})$ whose unit normal is $v_\alpha(\mathbf{y})$. The kernel functions in (19) are derived readily by the Stroh complex variable formalism. Consider a unit I component of

the extended line force at the point $\xi = y_1 + iy_2$; the resulting K component of the extended displacement $G_{KI}(z)$ at $z = x_1 + ix_2$ is given by

$$G_{KI}(z) = \Im \frac{1}{\pi} \sum_{N=1}^4 A_{KN} A_{IN} \ln(z_N - \xi_N), \quad (20)$$

where $z_N = x_1 + \eta_N x_2$ and $\xi_N = y_1 + \eta_N y_2$. Next consider a unit I component of the extended dislocation dipole at the point $\xi = y_1 + iy_2$ along a segment $d\xi = dy_1 + idy_2$ of length ds , which is a segment of the extended displacement discontinuity; the resulting K component of the extended displacement $H_{KI}(z)^* ds$ is given by

$$H_{KI}(z)^* ds = -\Im \frac{1}{\pi} \sum_{N=1}^4 A_{KN} L_{IN} \frac{d\xi_N}{z_N - \xi_N}, \quad (21)$$

where $d\xi_N = dy_1 + \eta_N dy_2$.

In the implementation of the BEM, the whole boundary is approximated by a collection of straight elements \sum_{Γ} and the extended displacement and traction on the boundary are approximated by quadratic interpolation functions.

The extended displacement contribution (U_I) from the single boundary element consists of the extended boundary displacement (U_I^U) and traction (U_I^T) contributions. For the straight element with the quadratic interpolation, each contribution can be evaluated analytically as given by Denda and Mansukh [40]. Analytical integration of the boundary integrals provides the simplicity in the BEM formulation, by removing the concern on the weak and the strong singularities of the boundary integrals, and improves the accuracy and the speed of the BEM.

4. Numerical Green's Function by Whole Crack Singular Element

In an infinite body consider a straight crack in the interval $(-1, +1)$ on the horizontal coordinate axis. Integration of (21) along the crack, where $\xi_N = \eta_1 \equiv \eta$ for all values of N ($= 1, 2, 3, 4$), will give the extended displacement

$$U_J^{(d)}(x_1, x_2) = \Im \frac{1}{\pi} \int_{-1}^{+1} \sum_{N=1}^4 A_{JN} \sum_{K=1}^3 L_{KN} \delta_K(\eta) \frac{d\eta}{\eta - z_N}. \quad (22)$$

Interpolate the extended crack opening displacement (COD) by

$$\delta_K(\eta) = \sqrt{1 - \eta^2} \sum_{m=1}^M \delta_K^{(m)} U_{m-1}(\eta) \quad (23)$$

where $U_{m-1}(\eta)$ is Chebyshev polynomial of the second kind. This will embed the \sqrt{r} behavior of the extended COD at the crack tips. The integral (22) with (23) can be evaluated analytically to give

$$U_J^{(d)}(x_1, x_2) = -\Im \sum_{m=1}^M \sum_{N=1}^4 A_{JN} \sum_{K=1}^4 L_{KN} \delta_K^{(m)} R_m(z_N), \quad (24)$$

where

$$R_m(z_N) = \left(z_N - \sqrt{(z_N)^2 - 1} \right)^m \quad (m \geq 1). \quad (25)$$

The extended stress function is similarly given by

$$\Phi_J^{(d)}(x_1, x_2) = -\Im \sum_{m=1}^M \sum_{N=1}^4 L_{JN} \sum_{K=1}^4 L_{KN} \delta_K^{(m)} R_m(z_N). \quad (26)$$

The extended displacement and the stress functions for the crack with half length a are still given by (24) and (26), respectively, if we replace the arguments z_α by the normalized arguments $Z_\alpha = z_\alpha/a$. The extended stress components are obtained by substituting the extended stress function thus obtained into (16) with the result

$$\begin{aligned} \Sigma_{2J}^{(d)}(x_1, x_2) &= -\frac{1}{a} \Im \sum_{m=1}^M \sum_{N=1}^4 L_{JN} \sum_{K=1}^4 L_{KN} \delta_K^{(m)} m G_{m-1}(Z_N), \\ \Sigma_{1J}^{(d)}(x_1, x_2) &= \frac{1}{a} \Im \sum_{m=1}^M \sum_{N=1}^4 \eta_M L_{JN} \sum_{K=1}^4 L_{KN} \delta_K^{(m)} m G_{m-1}(Z_N), \end{aligned} \quad (27)$$

where

$$G^{(m-1)}(Z_N) = -\frac{\left(Z_N - \sqrt{(Z_N)^2 - 1} \right)^m}{\sqrt{(Z_N)^2 - 1}} \quad (m \geq 1). \quad (28)$$

On the crack line we find the extended traction

$$T_J^\pm(X) = \pm \frac{1}{a} \Im \sum_{m=1}^M \sum_{N=1}^4 L_{JN} \sum_{K=1}^4 L_{KN} \delta_K^{(m)} m U_{m-1}(X) \quad (|X| \leq 1), \quad (29)$$

where $X = x_1/a$ and the superscripts $+$ and $-$ indicate limits from above and below the horizontal coordinate axis, respectively. In front of each crack tip at $X = \pm 1$ we find

$$K_J(\pm 1) = \sqrt{\frac{\pi}{a}} \Im \sum_{m=1}^M (\pm)^{m+1} \sum_{N=1}^4 L_{JN} \sum_{K=1}^4 L_{KN} \delta_K^{(m)} m, \quad (30)$$

which give Mode I ($K_I = K_2$), Mode II ($K_{II} = K_1$), Mode III ($K_{III} = K_3$) and Mode IV ($K_{IV} = K_4$) extended stress intensity factors. The effect of the unit extended crack opening displacement component on the extended stress intensity factors is given by the influence coefficients defined by

$$K_{JI} = \sqrt{\frac{\pi}{a}} \Im \sum_{N=1}^4 L_{JN} L_{IN}, \quad (31)$$

where K_{JI} is K_J due to the unit crack opening displacement component δ_I .

For each mode m of crack opening displacement defined by (23), equations (24) and (26) give the influence functions for the extended displacement and stress function components in the sense that the crack opening displacement and the stress singularity are built in. Given the arbitrary non-zero value of the crack face extended traction, formula (29) is used to determine the magnitude $\delta_k^{(m)}$ of the influence functions. The linear combination of these influence functions, (23), with numerically determined values of $\delta_k^{(m)}$ defines the numerical Green's functions for the problem. These Green's functions are more flexible than the traditional analytical Green's functions since any non-zero extended traction boundary condition can be incorporated. Once the extended COD is determined the formula (30) gives the extended SIFs in terms of $\delta_k^{(m)}$. There is no need for the post-processing. The crack element developed here is called the whole crack singular element (WCSE), which serves as the basis of the numerical Green's functions that can be extended to multiple cracks in the finite domain with the introduction of the boundary elements.

For the impermeable crack the crack surface electric induction is zero (i.e., $D_2^c = 0$), but this is nonzero for the permeable and semipermeable cracks. The solution strategies for the impermeable and permeable cracks are summarized as follows. (1) For the impermeable crack set all four traction components zero ($T_I^c = 0; I = 1, 2, 3, 4$) and solve for four components ($\delta_I; I = 1, 2, 3, 4$) of the extended COD. (2) For the permeable crack set the three traction components and the electric potential jump to zero ($T_I^c = 0; I = 1, 2, 3$ and $\delta_4 = 0$) and solve for the three components of the COD and the electric induction ($\delta_I; I = 1, 3$ and T_4^c). Notice that Both (1) and (2) are linear procedures with four equations for four unknowns at each crack surface point that can be solved by the BEM. However, the semipermeable crack has five unknowns ($\delta_I; I = 1, 2, 3, 4$ and T_4^c) that require a nonlinear iterative solution procedure introduced later.

5. Upper and Lower Bound Analysis

Wang and Mai [37] and Gruebner et al. [38], in their FEM analysis of the single crack, have shown that the impermeable and the permeable cracks set the bounds for the semipermeable crack. The linear BEM solution procedures for these cracks established in this section will be used in the nonlinear iterative solution procedure for the semipermeable cracks later on. Consider a straight crack in a finite body subject to the extended boundary displacement $\{\mathbf{U}\}$ and traction $\{\mathbf{T}\}$ vectors. For the crack define the local coordinate system with its origin at the crack center and the horizontal

axis along the crack and interpolate the extended COD by M Chebyshev polynomials in (23). This introduces a $4M$ - dimensional COD vector $\{\delta\}$ for the impermeable crack, which is determined by setting the extended traction at M collocation points on the crack surface to zero as follows:

$$\{\mathbf{T}^c\} = [\mathbf{H}^c]\{\mathbf{U}\} + [\mathbf{G}^c]\{\mathbf{T}\} + [\mathbf{D}^c]\{\delta\} = \{\mathbf{0}\}, \quad (32)$$

where $\{\mathbf{T}^c\}$ is $4M$ - dimensional global extended traction on the impermeable crack and the coefficient matrices $[\mathbf{H}^c]$, $[\mathbf{G}^c]$ and $[\mathbf{D}^c]$ represent contributions from the extended boundary displacement, traction and COD $\{\delta\}$ of the crack, respectively.

For the permeable crack introduce a new four-dimensional unknown vector $\delta^* = (\delta_1, \delta_2, \delta_3, T_4^c)$ by replacing the fourth component of the extended COD, $\delta_4 = 0$, with the unknown crack surface electric induction, $T_4^c = -D_2^c$ defined on the upper face of the crack with the negative unit normal. The exchange of δ_4 and T_4^c in (32) will produce a new modified system of equations for the new unknowns $\delta^* = (\delta_1, \delta_2, \delta_3, T_4^c)$, which is the routine procedure in the standard BEM in applying the displacement boundary conditions in elasticity.

An additional system of extended boundary displacement equations needed to solve for the non-crack extended boundary displacement and traction is given by

$$\{\mathbf{u}\} = [\mathbf{H}]\{\mathbf{U}\} + [\mathbf{G}]\{\mathbf{T}\} + [\mathbf{D}]\{\delta\}, \quad (33)$$

where coefficient matrices $[\mathbf{H}]$, $[\mathbf{G}]$ and $[\mathbf{D}]$ represent contributions from the extended boundary displacement, traction and crack. Notice that the extended COD for the permeable crack in (33) has only three components since $\delta_4 = 0$.

Although the collocation point on the crack surface can be selected arbitrarily, the best result is obtained by including the crack tips among the collocation points. Notice that the local contributions from the crack must be converted to the global components before adding them for all cracks. For the impermeable cracks, the system of equations, (32) and (33), determines the extended COD vector $\{\delta\}$ and the unknown extended boundary displacement and traction components. For the permeable cracks, the modified version of equation (32) involving the modified unknowns $\delta^* = (\delta_1, \delta_2, \delta_3, T_4^c)$ along with equation (33) should be used. The stress intensity factors are calculated directly by the formula (30) in terms of $\delta_k^{(m)}$ without the additional post-processing. Numerical results for the upper and lower bounds of the extended stress intensity factors for multiple crack configurations are reported by Denda and Mansukh [40].

6. Semipermeable Cracks

6.1. Analytical solution for the semipermeable BC

Consider a single horizontal semipermeable crack in an infinite piezoelectric domain with the remote loading $T_I^\infty = \sigma_{I2}^\infty = (\sigma_{12}^\infty, \sigma_{22}^\infty, \sigma_{32}^\infty, D_2^\infty)$ and the crack surface loading $(T_I^c)^+ = -\sigma_{I2}^c = -(0, 0, 0, D_2^c)$, where $(T_4^c)^+ = -D_2^c$ on the upper crack surface. Using the superposition principle, the crack surface traction boundary condition is given by

$$(T_I)^+ = -(\sigma_{I2}^\infty - \sigma_{I2}^c), \quad (34)$$

where the left hand side is given by (29). The final solution is obtained by superposing the solution of the loaded infinite plain without the crack. For the semipermeable crack the crack surface electric induction is nonzero (i.e., $D_2^c \neq 0$). Consider the single horizontal crack of length $2a$ in an infinite body subject to the boundary condition (34). One can show (Denda and Mansukh [40]) that the crack opening displacement δ_I ($I = 1, 2, 3, 4$) is given by

$$\delta_I = H_{IJ} (\sigma_{J2}^\infty - \sigma_{J2}^c) \sqrt{a^2 - x_1^2}, \quad (35)$$

where H_{IJ} is the compliance matrix defined by

$$H_{IJ} = -2\Im \left(A_{IK} L_{KJ}^{-1} \right), \quad (36)$$

where L_{KJ}^{-1} is the inverse of L_{KJ} . The value of D_2^c for the semipermeable crack is given, from (3), by

$$D_2^c = -\varepsilon_c \frac{H_{41}\sigma_{12}^\infty + H_{42}\sigma_{22}^\infty + H_{43}\sigma_{32}^\infty + H_{44}(D_2^\infty - D_2^c)}{H_{21}\sigma_{12}^\infty + H_{22}\sigma_{22}^\infty + H_{23}\sigma_{32}^\infty + H_{24}(D_2^\infty - D_2^c)}. \quad (37)$$

Solving for D_2^c we get

$$D_2^c = \frac{\sum_{J=1}^4 H_{2J}\sigma_{2J}^\infty - \varepsilon_c H_{44} \pm \sqrt{(\sum_{J=1}^4 H_{2J}\sigma_{2J}^\infty - \varepsilon_c H_{44})^2 + 4\varepsilon_c H_{24} \sum_{J=1}^4 H_{4J}\sigma_{2J}^\infty}}{2H_{24}}, \quad (38)$$

when $H_{24} \neq 0$ and

$$D_2^c = -\varepsilon_c \frac{\sum_{J=1}^4 H_{4J}\sigma_{2J}^\infty}{\sum_{J=1}^4 H_{2J}\sigma_{2J}^\infty - \varepsilon_c H_{44}}, \quad (39)$$

when $H_{24} = 0$. In (38) we select the branch that gives the positive crack opening displacement δ_2 . Note that H_{24} is the measure of coupling between the crack opening δ_2 and the electric potential jump δ_4 and depends on the material constants.

6.2. Numerical solution procedure

For the impermeable crack $\delta_4 \neq 0$ and $T_4 = 0$, while for the permeable crack $\delta_4 = 0$ and $T_4 \neq 0$. Knowing that the semipermeable crack solution is somewhere in between the impermeable and permeable crack solutions, we suggest the following iteration procedure for the semipermeable single crack:

1. Get the impermeable solution $\delta_4^{[0]}$ using the impermeable BEM solver.
2. (a) Set $\delta_4^{[1]} = p^{[1]} * \delta_4^{[0]}$ for a slightly reduced value of $\delta_4^{[1]}$ given by a control parameter $p = p^{[1]} < 1.0$,
 - (b) Calculate, using the permeable BEM solver, the crack opening $\delta_2^{[1]}$ and the electric induction $D_2^{c[1]} = -T_4^{c[1]}$ based on the set value $\delta_4^{[1]}$ of the electric potential.
 - (c) Calculate $\epsilon_c^{[1]} = -D_2^{c[1]} \frac{\delta_2^{[1]}}{\delta_4^{[1]}}$.
3. Repeat STEP 2 for progressively reduced values of $\delta_4^{[i]} = p^{[i]} * \delta_4^{(0)}$ for the control parameter $p = p^{[i]} (i = 2, 3, 4, \dots)$ to plot $\delta_4^{[i]} - \epsilon_c^{[i]}$ curve.
4. Intersection of the $\delta_4^{[i]} - \epsilon_c^{[i]}$ curve obtained in STEP 3 and the horizontal line $\epsilon_c^{[i]} = \epsilon_{air}$ gives the semipermeable solution $\delta_4^{(sp)}$.

For the crack in the infinite body the extended crack opening displacement is given exactly by one term of the interpolation (i.e., $M = 1$ in (23)),

$$\delta_k(\eta) = \sqrt{1 - \eta^2} \delta_k^{(1)} U_0(\eta), \quad (40)$$

where $U_0 = 1$. Thus the ratio of δ_2/δ_4 , used in the iteration, is constant $\delta_2^{(1)}/\delta_4^{(1)}$ over the entire crack surface. This feature guarantees that the electric induction on the crack surface is also constant over the surface. During the iteration it is sufficient to sample them at a single point on the crack, typically at the center. In contrast to this, the interpolation of the extended crack opening displacement for the crack in the finite body requires multiple polynomial terms $U_{m-1}(\eta)$ as in (23). Consequently the ratio

$$\frac{\delta_2}{\delta_4} = \frac{\sum_{m=1}^M \delta_2^{(m)} U_{m-1}(\eta)}{\sum_{m=1}^M \delta_4^{(m)} U_{m-1}(\eta)} \quad (41)$$

is not constant over the crack surface. In calculating the ϵ_c , we suggest to evaluate it at M discrete points on the crack and take the average. These sample points coincides with M collocation points

used by the permeable solver. In the proposed iteration process, the amplitude of the electric potential jump is varied gradually from the impermeable to the permeable condition, while its mode is fixed.

6.3. Material constants and Loading

Material constants we need are the elastic compliance at constant electric induction (s_{ijkl}^D), piezoelectric strain (g_{kij}), and dielectric impermeability constants at constant stress (β_{ik}^σ), while only the elastic stiffness (c_{ijkl}^E) at constant electric field, piezoelectric stress (e_{ikl}), and dielectric permittivity constants at constant strain (κ_{ik}^ε) are available in literature [44]. Thus, we use the input ($c_{ijkl}^E, e_{ikl}, \kappa_{ik}^\varepsilon$) and calculate ($s_{ijkl}^D, g_{kij}, \beta_{ik}^\sigma$) following Denda and Mansukh [40]. Notice that the elastic stiffness, the piezoelectric stress and the dielectric permittivity constants are of the order of 10^{11} (N/m^2), 10^1 (C/m^2) and 10^{-9} ($C/(mV)$), respectively, ranging from extremely large to extremely small. The strain and the electric fields are of the order of 10^{-3} and 10^7 (V/m), respectively. Their normalization is essential to avoid truncation errors due to the wide variation of the order of magnitudes. For a typical constant or variable q , select its reference value q_0 and normalize the former by introducing a non-dimensional quantity $\bar{q} = q/q_0$. The reference values selected for the stress, strain, electric induction, and the electric fields are $\sigma_0 = 10^8$ (N/m^2), $\epsilon_0 = 10^{-3}$, $D_0 = 10^{-2}$ (C/m^2), and $E_0 = 10^7$ (V/m), respectively. The reference values of other quantities can be determined in terms of these four reference variables in order to keep the normalized governing equations in exactly the same form as the original equations. For example the reference values of the extended stress intensity factors are $K_{I0} = K_{II0} = K_{III0} = 10^{13/2}x_0^{1/2}(N/m^{3/2})$ and $K_{IV0} = 10^{-7/2}x_0^{1/2}(C/m^{3/2})$, where $x_0(m)$ is the characteristic length of the problem. See Table 1 for a list of the reference values, where $x_0(m)$ is the characteristic length of the problem. In this paper $x_0 = 1(m)$ is used.

Let a_i ($i = 1, 2, 3$) be the material coordinate axes, taken along the crystal lattice directions, in which the material constants are defined and let x_i be the spatial coordinate axes. To see different material symmetry we rotate the material axes relative to the spacial axes. In the System 12, the material axes coincide with the spacial axes so that $x_1 = a_1, x_2 = a_2, x_3 = a_3$. In the System 23, we have $x_1 = a_2, x_2 = a_3, x_3 = a_1$. In Systems 12 and 23 the two-dimensional x_1x_2 plane is selected to be a_1a_2 and a_2a_3 , respectively. While the input data for System 12 need no modification, those for System 23 need to be modified following the cyclic transformation of indices. The material constants for the piezoelectric material, in System 12, used in this paper are for Barium Sodium

Table 1: Reference values for material constants and field variables in piezoelectricity.

Displacement	$u_0 = x_0 \epsilon_0 = 10^{-3} x_0$ (m)	Elec. Potential	$\phi_0 = x_0 E_0 = 10^7 x_0$ (V)
Stiffness	$c_0 = \frac{\sigma_0}{\epsilon_0} = 10^{11}$ (N/m ²)	Permittivity	$\epsilon_0 = \frac{D_0}{E_0} = 10^{-9}$ (C/(mV))
Compliance	$s_0 = \frac{\epsilon_0}{\sigma_0} = 10^{-11}$ (m ² /N)	Impermeability	$\beta_0 = \frac{E_0}{D_0} = 10^9$ (mV/C)
Piezoelectric	$e_0 = \frac{\sigma_0}{E_0} = 10^1$ (N/(mV))	Piezoelectric	$g_0 = \frac{E_0}{\sigma_0} = 10^{-1}$ (mV/N)
Stress Constant	$= \frac{D_0}{\epsilon_0} = 10^1$ (C/m ²)	Strain Constant	$= \frac{\epsilon_0}{D_0} = 10^{-1}$ (m ² /C)

Niobate($Ba_2NaNb_5O_{15}$, Orthogonal $2mm$):

$$\begin{aligned}
 [c_{\mathcal{I}\mathcal{J}}^E/c_r] &= \begin{bmatrix} 23.9, & 10.4, & 5.0, & 0.0, & 0.0, & 0.0 \\ & 24.7, & 5.2, & 0.0, & 0.0, & 0.0 \\ & & 13.5, & 0.0, & 0.0, & 0.0 \\ & & & 6.5, & 0.0, & 0.0 \\ & & & & 6.6, & 0.0 \\ & & & & & 7.6 \end{bmatrix}, \\
 [e_{i\mathcal{J}}/e_r] &= \begin{bmatrix} 0.0, & 0.0, & 0.0, & 0.0, & 2.8, & 0.0 \\ 0.0, & 0.0, & 0.0, & 3.4, & 0.0, & 0.0 \\ -0.4, & -0.3, & 4.3, & 0.0, & 0.0, & 0.0 \end{bmatrix}, \\
 [\kappa_{ij}^\epsilon/\epsilon_r] &= \begin{bmatrix} 222.0, & 0.0, & 0.0 \\ & 227.0, & 0.0 \\ & & 32.0 \end{bmatrix}. \tag{42}
 \end{aligned}$$

The uppercase and lowercase Roman indices range from 1 to 6 and 1 to 3, respectively and $c_r = 10^{10}$ (N/m²), $e_r = 1.0$ (C/m²) and $\epsilon_r = 8.854 \times 10^{-12}$ (farads/m). Only the upper triangular half of the symmetric matrices are shown.

We consider BSN System 12, BSN System 23. BSN System 12 has the electrical/out-of-plane mechanical coupling with no in-plane/out-of-plane mechanical and electrical/in-plane mechanical couplings (Denda and Mansukh [40]). Its influence coefficients, defined by (31), are given by

$$[K_{JI}] = \begin{bmatrix} 0.900143, & 0.0, & 0, & 0.0 \\ 0.0, & 0.915084, & 0.0, & 0.0 \\ 0.0, & 0.0, & 0.580679, & 0.274588 \\ 0.0, & 0.0, & 0.274588, & -1.7619 \end{bmatrix}, \tag{43}$$

which are normalized according to the guideline described earlier. Notice that K_{11} (or K_{22}) is the stress intensity factor K_{II} (or K_I) due to the unit crack opening displacement component δ_1 (or δ_2). Non-zero off diagonal components K_{34} and K_{43} indicate the electrical/out-of-plane mechanical coupling. The coefficient H_{24} , defined 36, is zero (i.e., $H_{24} = 0$). BSN System 23 has the electrical/in-plane mechanical coupling with no in-plane/out-of-plane mechanical and electrical/out-of-plane mechanical couplings (Denda and Mansukh [40]) with the influence coefficients given by

$$[K_{JI}] = \begin{bmatrix} 0.884093, & 0.0, & 0, & 0.0 \\ 0.0, & 0.637451, & 0.0, & 0.211767 \\ 0.0, & 0.0, & 0.6276599, & 0.0 \\ 0.0, & 0.211767, & 0.0, & -0.811889 \end{bmatrix} \quad (44)$$

and $H_{24} \neq 0$.

6.4. Numerical results

The proposed algorithm was applied to a single horizontal crack (half crack length $\bar{a} = 1$) in the infinite BSN System 12, which has the electrical/out-of-plane mechanical coupling with no in-plane/out-of-plane mechanical and electrical/in-plane mechanical couplings. The remote loading components considered are $\bar{\sigma}_{22}^\infty = \sigma_{22}^\infty/\sigma_0 = 1$ (tension) and $\bar{D}_2^\infty = D_2^\infty/D_0 = 1$ (electric induction), where $\sigma_0 = 10^8(N/m^2)$ and $D_0 = 10^{-2}C/m^2$. The remote loading is selected to produce both δ_2 (opening) and δ_4 (potential jump) at the same time. Due to the absence of the electrical/in-plane mechanical couplings, the load $\bar{\sigma}_{22}^\infty$ does not produce δ_4 for the impermeable crack. Under this loading both the impermeable and permeable boundary conditions produce zero potential, and consequently, zero electric induction in the opened crack. This is perfectly consistent in the air filling the crack since, even though the permittivity of the air is not zero, the zero electric potential makes the electric and the electric induction fields zero in the air. In order to produce non-zero δ_4 , it is necessary to apply the additional loading, \bar{D}_2^∞ . Similarly, the solo application of the load \bar{D}_2^∞ produces only δ_4 , but not δ_2 . Although the impermeable and permeable boundary conditions produce different electric induction on the crack faces, both solutions are consistent and there is no need to come up with the semipermeable boundary condition. The numerical analysis was performed entirely in terms of the normalized quantities and all numerical results are normalized. The iteration was performed 1000 times by decreasing the parameter p evenly. Figure 1 (a) shows the variation of $\bar{\epsilon}_c$ as the function of the control parameter p . The intersection of this curve with the horizontal line $\bar{\epsilon}_{air} = 8.854$ occurs at $p^{(smp)} = 0.189292$. Figures 1 (b) and (c) show variation of \bar{K}_{IV} ,

\bar{D}_2^c , respectively. They vary linearly between the impermeable and permeable conditions such that the semipermeable quantities are given by $\bar{K}_{IV}^{(smp)} = p^{(smp)} \bar{K}_{IV}^{(imp)}$ and $\bar{D}_2^{c(smp)} = (1-p^{(smp)}) \bar{D}_2^{c(per)}$, where $\bar{K}_{IV}^{(imp)} = \sqrt{\pi}$ and $\bar{D}_2^{c(per)} = 1$. The value of $\bar{D}_2^{c(smp)} = 0.810708$ agrees perfectly with the theoretical value $\bar{D}_4^{c(smp)} = 0.810709$ given by (39) for $H_{24} = 0$. Note that, as shown in Figure 1 (d), \bar{K}_{III} is very small, but not zero. Although not shown, \bar{K}_I and $\bar{\delta}_2$ remain constant throughout the iteration and \bar{K}_{II} is zero. Figures 2 (a) and (b) show the variation of (a) $\bar{\delta}_4$ and (b) \bar{D}_2^c along the crack for impermeable, semipermeable and permeable cracks, respectively.

Consider a single horizontal crack (half crack length $\bar{a} = 1$) in the infinite BSN System 23, which has the electrical/in-plane mechanical coupling with no in-plane/out-of-plane mechanical and electrical/out-of-plane mechanical couplings. The only remote loading component applied is $\bar{\sigma}_{22}^\infty = \sigma_{22}^\infty/\sigma_0 = 1$ (tension), which produces both δ_2 (opening) and δ_4 (potential jump) at the same time. Figure 3 (a) shows the variation of $\bar{\epsilon}_c$ as the function of the control parameter p . The intersection of this curve with the horizontal line $\bar{\epsilon}_{air} = 8.854$ occurs at $p^{(smp)} = 0.133934$. Figures 3 (b) and (c) show variation of \bar{K}_{IV} , \bar{D}_2^c , respectively. They vary linearly between the impermeable and permeable conditions such that the semipermeable quantities are given by $\bar{K}_{IV}^{(smp)} = p^{(smp)} \bar{K}_{IV}^{(imp)}$ and $\bar{D}_2^{c(smp)} = (1-p^{(smp)}) \bar{D}_2^{c(per)}$, where $\bar{K}_{IV}^{(imp)} = \sqrt{\pi}$ and $\bar{D}_2^{c(per)} = 1$. The value of $\bar{D}_2^{c(smp)} = -0.287713$ agrees perfectly with the theoretical value $\bar{D}_4^{c(smp)} = -0.287715$ given by (38) for $H_{24} \neq 0$. Note that, as shown in Figure 3 (d), \bar{K}_I varies linearly between impermeable and permeable cracks, in contrast to the BSN System 12 considered above for which K_I remains constant. Figures 4 (a) and (b) show the variation of (a) $\bar{\delta}_4$ and (b) $\bar{\delta}_2$ along the crack for impermeable, semipermeable and permeable cracks, respectively. Although not shown, \bar{D}_2^c for each of the three cracks is constant along the crack.

Consider a crack ($\bar{a} = 1$) in a finite BSN System 12 body ($\bar{H} = \bar{W} = 4$) under the unit normalized tension and electric induction, $\bar{\sigma}_{22} = 1$ (tension) and $\bar{D}_2 = 1$ (electric induction), as shown in Figure 5. The iteration has been applied to this crack using $M = 7$ terms in the interpolation (23) and the average value was used to calculate $\bar{\epsilon}_c$. Figure 6 shows the relative error in the $\bar{\epsilon}_c$ over the crack surface for the semipermeable solution. This figure confirms that the ratio (41) is indeed not constant over the crack. Although the proposed algorithm is not perfect, the $\bar{\epsilon}_c$ obtained by the proposed algorithm does not deviate more than 2 % from the required constant value $\bar{\epsilon}_{air}$ and good enough for the most of practical purposes. The semipermeable quantities are given by $\bar{K}_{IV}^{(smp)} = 0.441798$ and $\bar{D}_2^{c(smp)} = 0.779552$ using $p^{(smp)} = 0.220448$, $\bar{K}_{IV}^{(imp)} = 2.00409$ and $\bar{D}_2^{c(per)} = 1$. Figures 7 (a) and (b) show the electric potential jump and electric induction

field variations over the crack. Notice that, in the proposed iteration process, the amplitude of the electric potential jump is varied gradually from the impermeable to the permeable condition, while its mode is fixed. The constant electric induction value over the crack of the semipermeable crack, as shown in Figure 7 (b) is the consequent of this. The error in the $\bar{\epsilon}_c$, shown in Figure 6, indicates that the mode of the electric potential jump for the semipermeable crack is not the same as that for the impermeable crack and that the electric induction field may not be constant. The further modification of the proposed iteration needs to take into this mode change into consideration.

7. Concluding Remarks

A boundary element method (BEM) for the analysis of the semipermeable crack is developed using the numerical Green's function approach. The linear BEM solvers for the impermeable and permeable cracks are developed first and then an iterative procedure to reach the semipermeable solution using the impermeable and permeable solvers is proposed. Each step in the iteration requires the solution of the crack problem with a nonzero value of the electric induction in the crack. In the crack Green's function approach, the extended crack opening displacement (COD) of a straight crack is represented by the continuous distribution of extended dislocation dipoles, with the built-in \sqrt{r} COD behavior, which is integrated analytically to give the whole crack singular element (WCSE) equipped with the \sqrt{r} COD and the $1/\sqrt{r}$ crack tip extended stress singularity. In this approach the post-processing for the accurate determination of the extended stress intensity factors (SIFs) is not needed and is ideally suited for the proposed nonlinear iteration scheme for the semipermeable cracks. The analysis was performed for the single crack in the infinite and finite bodies successfully. The agreement with the analytical solution for the crack in the infinite body is perfect, while the solution for the crack in the finite body has a small but acceptable error.

The proposed iteration scheme can further be improved. Currently the parameter p is varied continuously from $p = 1$ (impermeable) to $p = 0$ (permeable). The method of bisection can replace this continuous tracking scheme, in which we divide the parameter interval into two and select the one that contains the semipermeable solution. The semipermeable solution obtained by the current scheme, whether by the continuous tracking or bisection, is very close to the exact solution, but it still contains some error in $\bar{\epsilon}_c$. This is due to the assumption of the fixed mode of electric potential jump. Improvement of the current algorithm to remove the existing error by allowing the mode

change of the electric potential is under investigation.

References

- [1] F. Narita, Y. Shindo, and K. Horiguchi. Electroelastic fracture mechanics of piezoelectric ceramics. In Y. Shindo, editor, *Mechanics of Electromagnetic Material Systems and Structures*, pages pp. 89–101, WIT Press, Southampton, 2002.
- [2] T.H. Hao and Z.Y. Shen. A new electric boundary condition of electric fracture mechanics and its applications. *Eng. Frac. Mech.*, Vol. 47:793–802, 1994.
- [3] W.F. Deeg. *The analysis of dislocation, crack and inclusion in piezoelectric solids*. PhD thesis, Stanford University, 1980.
- [4] H.A. Sosa and Y.E. Pak. Three-dimensional eigenfunction analysis of a crack in a piezoelectric material. *Int. J. Solids Struct.*, 26:1–15, 1990.
- [5] H.A. Sosa. Plane problems in piezoelectric media with defects. *Int. J. Solids Struct.*, 28:491–505, 1991.
- [6] H.A. Sosa. On the fracture mechanics of piezoelectric solids. *Int. J. Solids Struct.*, 29:2613–2622, 1992.
- [7] Y.E. Pak. Linear electro-elastic fracture mechanics of piezoelectric materials. *Int. J. Fract.*, 54:79–100, 1992.
- [8] P.B.Park and C.T. Sun. Effect of electric field on fracture of piezoelectric ceramics. *Int. J. Fract.*, 70:203–216, 1995.
- [9] P.B.Park and C.T. Sun. Fracture criteria for piezoelectric ceramics. *J. Am. Ceramic Soc.*, 78:1475–1480, 1995.
- [10] S. Kumar and R.N. Singh. Energy release rate and crack propagation in piezoelectric materials. part i: Mechanical/electrical load. *Acta Mater.*, 45:849–857, 1997.
- [11] S. Kumar and R.N. Singh. Energy release rate and crack propagation in piezoelectric materials. part ii: Combined mechanical and electrical loads. *Acta Mater.*, 45:859–868, 1997.

- [12] S. Kumar and R.N. Singh. Influence of applied electric field and mechanical boundary condition on the stress distribution at the crack tip in piezoelectric material. *Mater. Sci. Eng. A*, 231:1–9, 1997.
- [13] S. Kumar and R.N. Singh. Effect of mechanical boundary condition at the crack surfaces on the stress distribution at the crack tip in piezoelectric material. *Mater. Sci. Eng. A*, 231:64–77, 1998.
- [14] R.N. Singh and S. Kumar. Electromechanical response of cracks in piezoelectric materials under combined mechanical and electrical loadings. *Key Eng. Mater.*, 145-149:1005–1010, 1998.
- [15] Q.H. Qin and Y.W. Mai. A closed crack model for interface cracks in thermopiezoelectric materials. *Int. J. Solids Struct.*, 36:2463–2479, 1999.
- [16] Q.H. Qin. General solutions for thermopiezoelectrics with various holes under thermal loading. *Int. J. Solids Struct.*, 37:5561–5578, 2000.
- [17] B.L. Wang, J.C. Han, and S.Y. Du. Electroelastic fracture dynamics for multilayered piezoelectric materials under dynamic anti-plane shearing. *Int. J. Solids Struct.*, 37:4969–4986, 2000.
- [18] B.L. Wang and N. Noda. Mixed mode crack initiation in piezoelectric ceramic strip. *Theoret. Appl. Fract. Mech.*, 34:35–47, 2000.
- [19] B.L. Wang and N. Noda. Axisymmetric deformation of piezoelectric multilayers. *Phil. Mag. A*, 81(4):1009–1019, 2001.
- [20] H. Gao and D.M. Barnett. An invariance property of local energy release rate in a strip saturation model of piezoelectric fracture. *Int. J. Fract.*, 79:R-25–R29, 1996.
- [21] C.C. Fulton and H. Gao. Electrical nonlinearity in fracture of piezoelectric ceramics. *Appl. Mech. Rev.*, 50(11):556–563, 1997.
- [22] H. Gao, T.Y. Zhang, and Tong P. Local and global energy release rate for an electrically yielded crack in a piezoelectric ceramic. *J. Mech. Phys. Solids*, 45:491–510, 1997.
- [23] K.P. Herrmann, V.V. Loboda, and V.B. Govorukha. On contact zone model for an electrically impermeable interface crack in a piezoelectric bimaterial. *Int. J. Fract.*, 111:203–227, 2001.

- [24] R.N. McMeeking. Electrostrictive stresses near crack-like flaws. *J. Appl. Math. Phys.*, 40:615–627, 1989.
- [25] G.K. Mikahailov and V.Z. Parton. *Electromagnetoelasticity*. Hemisphere, New York, 1990.
- [26] S.M. Kwon and K.Y. Lee. Analysis of stress and electric fields in a rectangular piezoelectric body with a center crack under anti-plane shear loading. *Int. J. Solids Struct.*, 37:4859–4869, 2000.
- [27] Y. Shindo, E. Ozawa, and J.P. Nowacki. Singular stress and electric fields of a cracked piezoelectric strip. *Int. J. Appl. Electromagn. Mater.*, 1:77–87, 1990.
- [28] Y. Shindo, K. Watanabe, and F. Narita. Electroelastic analysis of a piezoelectric ceramic strip with a central crack. *Int. J. Eng. Sci.*, 38:1–19, 2000.
- [29] M.L. Dunn. The effects of crack face boundary conditions on the fracture of piezoelectric solids. *Eng. Fract. Mech.*, 48:25–39, 1994.
- [30] T.Y. Zhang and P. Tong. Fracture mechanics for a mode-iii crack in a piezoelectric material. *Int. J. Solids Struct.*, 33:343–359, 1996.
- [31] C.F. Gao and W.X. Fan. Exact solutions for the plane problem in piezoelectric materials with an elliptic or a crack. *Int. J. Solids Struct.*, 36:2527–2540, 1999.
- [32] R.M. McMeeking. Crack tip energy release rate for a piezoelectric compact tension specimen. *Eng. Fract. Mech.*, 64:217–244, 1999.
- [33] B.J. Wang, J.C. Han, and S.Y. Du. New considerations for the fracture of piezoelectric materials under electromechanical loading. *Mech. Res. Commun.*, 27:435–444, 2000.
- [34] C.C. Fulton and H. Gao. Effect of local polarization on piezoelectric fracture. *J. Mech. Phys. Solids*, 49:927–952, 2001.
- [35] R.M. McMeeking. Towards a fracture mechanics for brittle piezoelectric and dielectric materials. *Int. J. Fract.*, 108:25–41, 2001.
- [36] T.Y. Zhang, M. Zhao, and P. Tong. Fracture of piezoelectric ceramics. *Advance in Applied Mechanics*, 38:148–289, 2001.

- [37] B.L. Wang and Y.W. Mai. On the electrical boundary conditions on the crack surfaces in piezoelectric ceramics. *Int. J. Eng. Sci.*, 41:633–652, 2003.
- [38] O. Gruebner, M. Kamlah, and D. Munz. Finite element analysis of cracks in piezoelectric materials taking into account the permittivity of the crack medium. *Engng. Frac. Mech.*, 70:1399–1413, 2003.
- [39] T.Y. Zhang, C.F. Qian, and P. Tong. Linear electro-elastic analysis of a cavity or a crack in a piezoelectric material. *Int. J. Solids Struct.*, 35:2122–2149, 1998.
- [40] M. M. Denda and M. Mansukh. Upper and lower bounds analysis of electric induction intensity factors for multiple piezoelectric cracks by the BEM (submitted). *Engng. Anal. with Boundary Elements*, 29:533–550, 2005.

FIGURE CAPTIONS

- Fig. 1.** Variation of (a) $\bar{\epsilon}_c$, (b) \bar{K}_{IV} , (c) \bar{T}_4^c and (d) \bar{K}_{III} in the iteration when p is varied from 1 to 0 for BSN System 12 under $\bar{\sigma}_{22}^\infty = 1$ (tension) and $\bar{D}_2^\infty = 1$ (electric induction).
- Fig. 2.** Variation of (a) $\bar{\delta}_4$ and (b) \bar{T}_4^c along the crack for impermeable, semipermeable and permeable cracks for BSN System 12 under $\bar{\sigma}_{22}^\infty = 1$ (tension) and $\bar{D}_2^\infty = 1$ (electric induction).
- Fig. 3.** Variation of (a) $\bar{\epsilon}_c$, (b) \bar{K}_{IV} , (c) \bar{D}_2^c and (d) \bar{K}_I in the iteration when p is varied from 1 to 0 for BSN System 23 under $\bar{\sigma}_{22}^\infty = 1$ (tension).
- Fig. 4.** Variation of (a) $\bar{\delta}_4$ and (b) $\bar{\delta}_2^c$ along the crack for impermeable, semipermeable and permeable cracks for BSN System 23 under $\bar{\sigma}_{22}^\infty = 1$ (tension).
- Fig. 5.** A center crack in a finite body under uniaxial tension and electric induction.
- Fig. 6.** Relative error in ϵ_c over the semipermeable crack surface for a crack in a finite body (Figure 5) under uniaxial tension and electric induction.
- Fig. 7.** Variation of (a) $\bar{\delta}_4$ and (b) \bar{D}_2^c over impermeable, semipermeable and permeable conditions for a crack in a finite body (Figure 5) under uniaxial tension and electric induction.

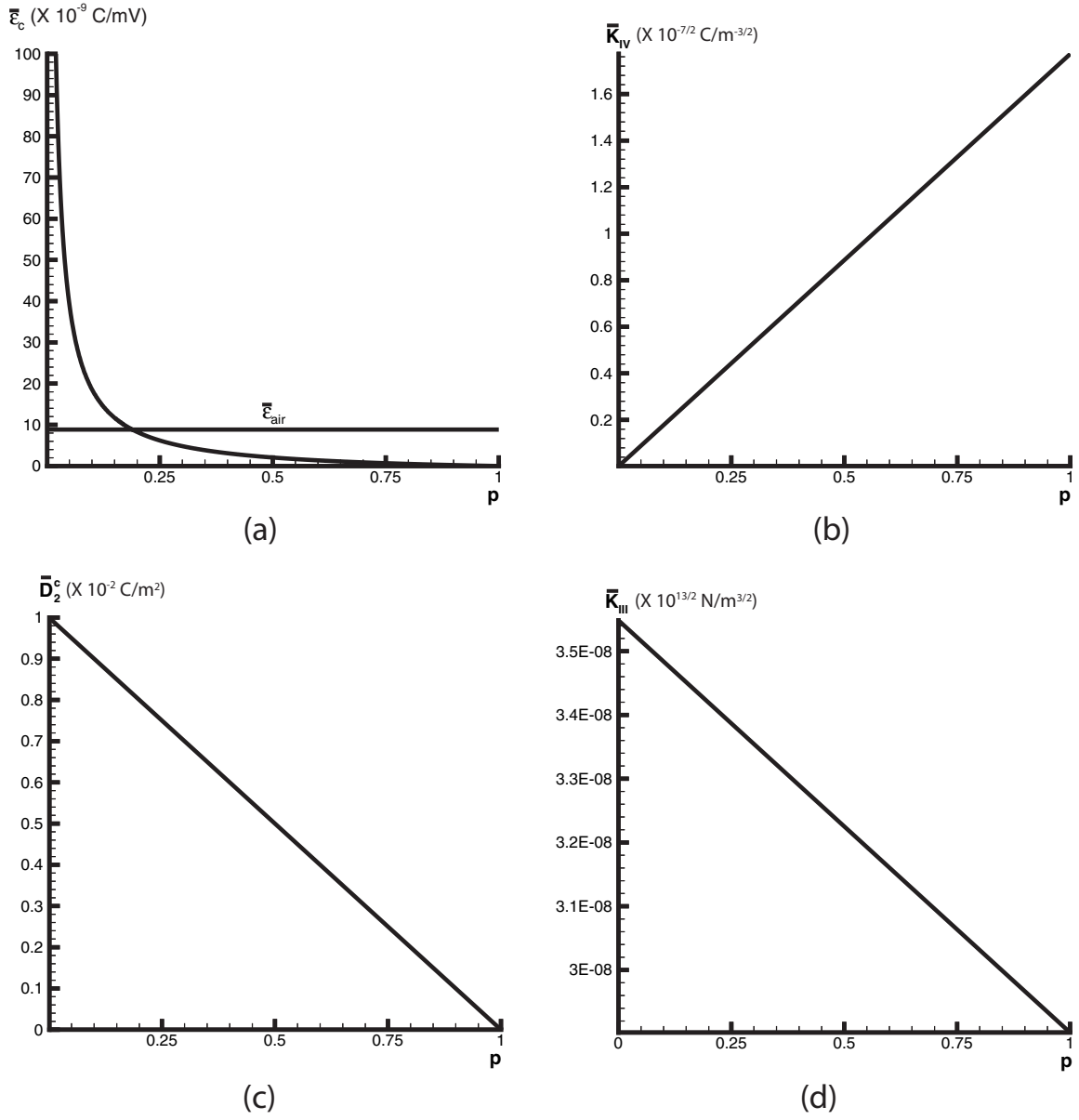


Figure 1: Variation of (a) $\bar{\epsilon}_c$, (b) \bar{K}_{IV} , (c) \bar{D}_2^c and (d) \bar{K}_{III} in the iteration when p is varied from 1 to 0 for BSN System 12 under $\bar{\sigma}_{22}^\infty = 1$ (tension) and $\bar{D}_2^\infty = 1$ (electric induction).

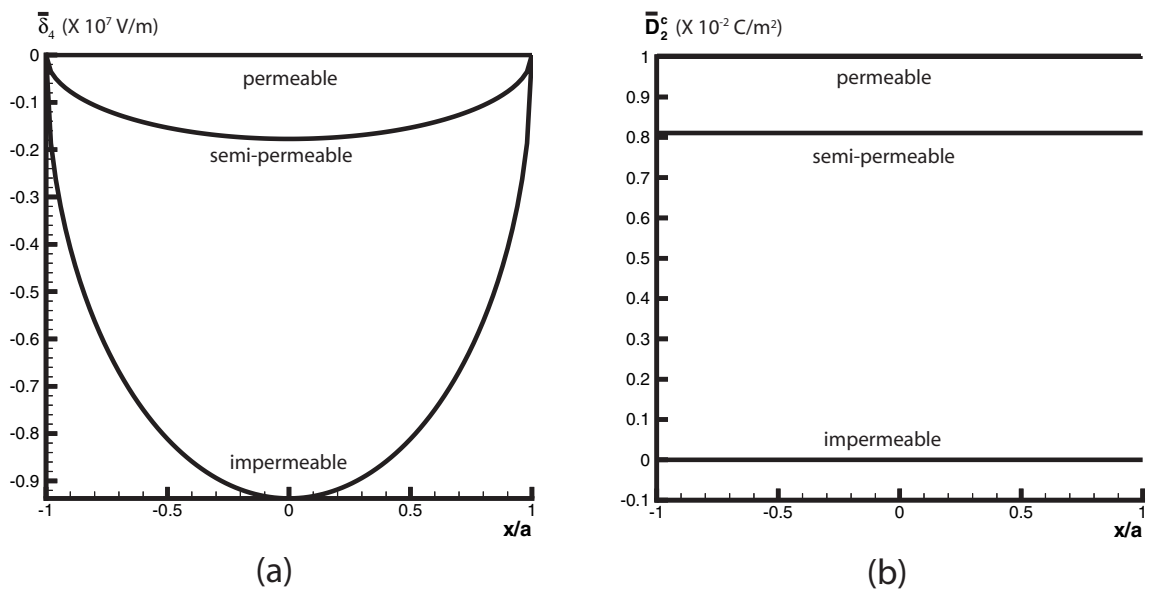


Figure 2: Variation of (a) $\bar{\delta}_4$ and (b) \bar{D}_2^c along the crack for impermeable, semipermeable and permeable cracks for BSN System 12 under $\bar{\sigma}_{22}^\infty = 1$ (tension) and $\bar{D}_2^\infty = 1$ (electric induction).

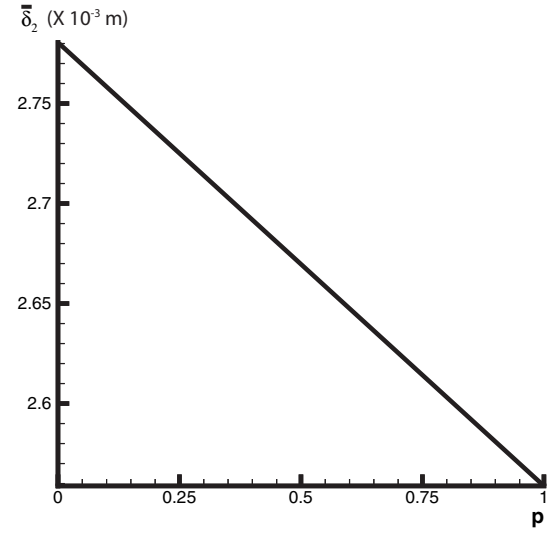
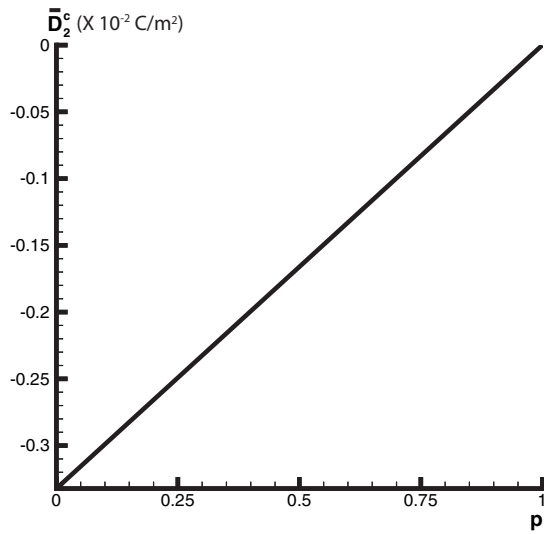
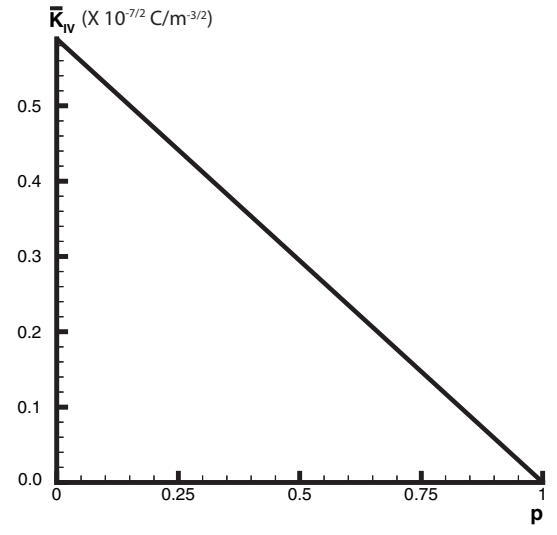
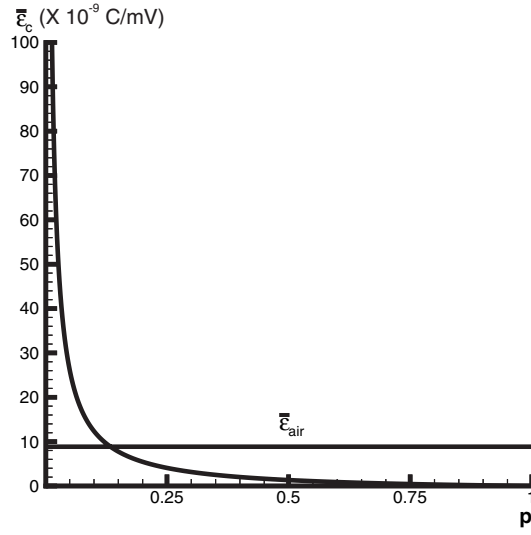


Figure 3: Variation of (a) $\bar{\epsilon}_c$, (b) \bar{K}_{IV} , (c) \bar{D}_2° and (d) \bar{K}_I in the iteration when p is varied from 1 to 0 for BSN System 23 under $\bar{\sigma}_{22}^{\infty} = 1$ (tension).

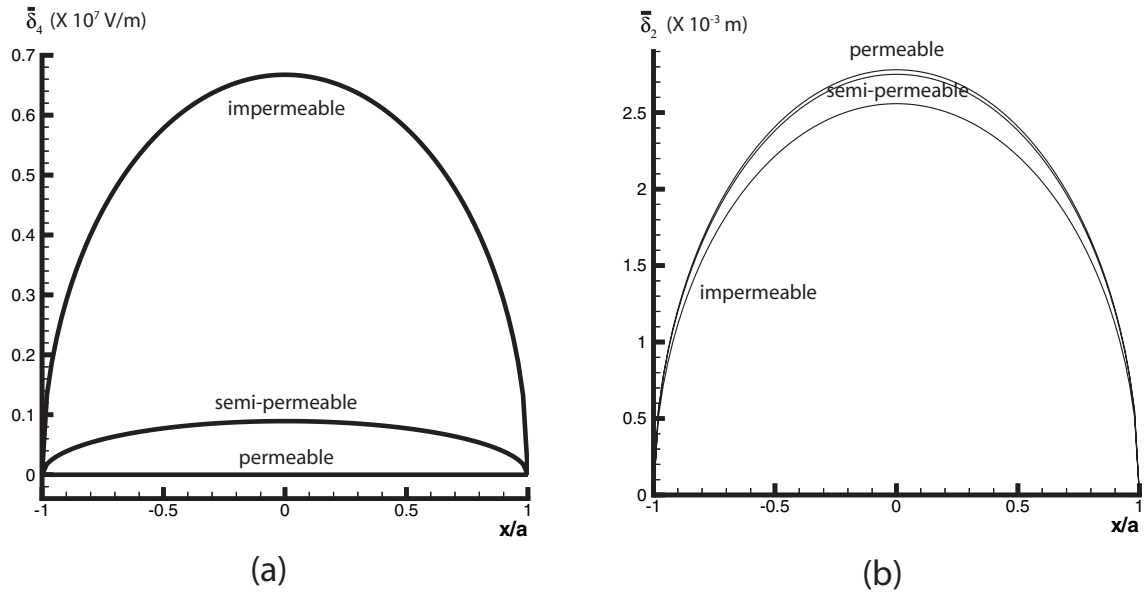


Figure 4: Variation of (a) $\bar{\delta}_4$ and (b) $\bar{\delta}_2^c$ along the crack for impermeable, semipermeable and permeable cracks for BSN System 23 under $\bar{\sigma}_{22}^\infty = 1$ (tension).

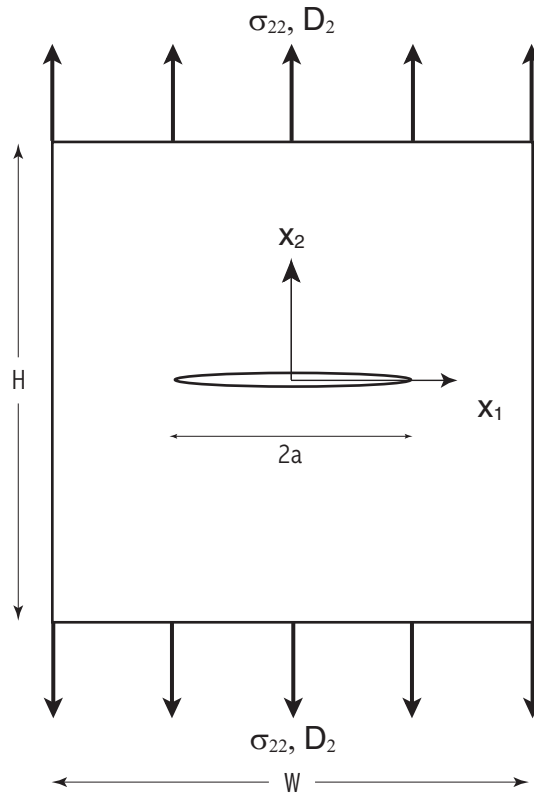


Figure 5: A center crack in a finite body under uniaxial tension and electric induction.

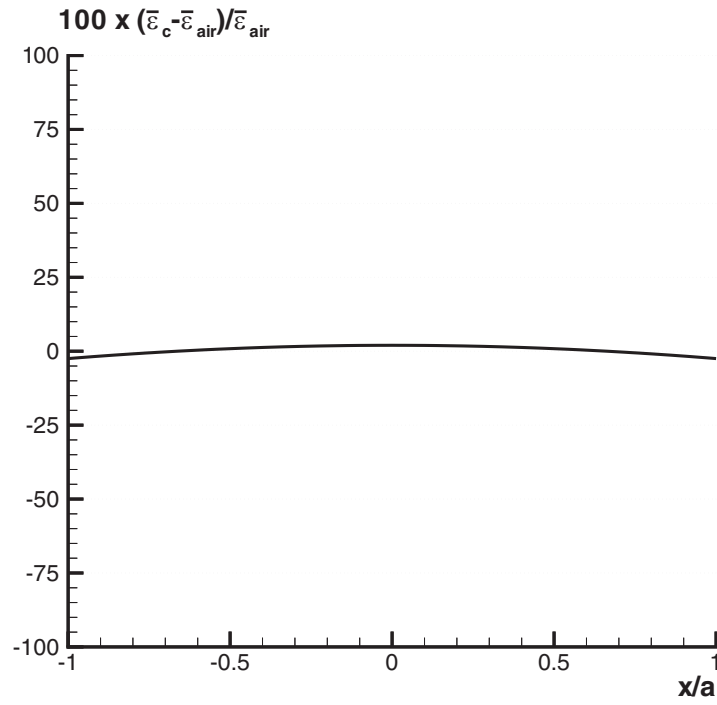


Figure 6: Relative error in $\bar{\epsilon}_c$ over the semipermeable crack surface for a crack in a finite body (Figure 5) under uniaxial tension and electric induction.

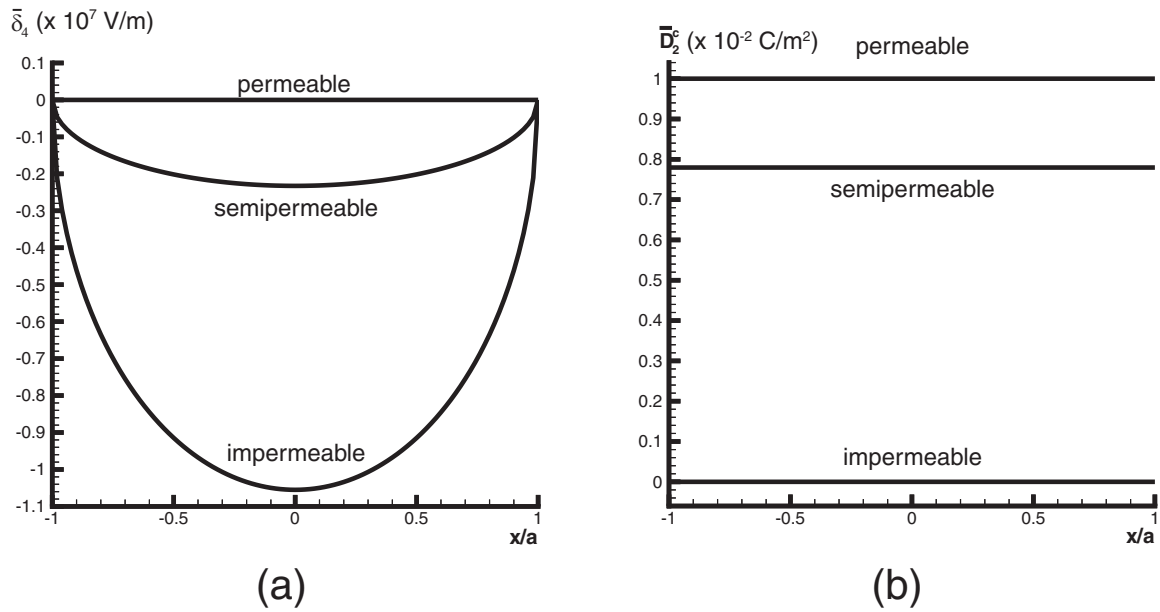


Figure 7: Variation of (a) $\bar{\delta}_4$ and (b) \bar{D}_2^ξ over impermeable, semipermeable and permeable conditions for a crack in a finite body (Figure 5) under uniaxial tension and electric induction.